EXPERIMENTS ON SCALAR DISPERSION WITHIN A MODEL PLANT CANOPY PART I: THE TURBULENCE STRUCTURE

M. R. RAUPACH, P. A COPPIN, and B. J. LEGG[1]

CSIRO Division of Environmental Mechanics, Canberra, ACT, Australia

(Received in final form 21 June, 1985)

Abstract. This is the first of a series of three papers describing experiments on the dispersion of trace heat from elevated line and plane sources within a model plant canopy in a wind tunnel. Here we consider the wind field and turbulence structure. The model canopy consisted of bluff elements 60 mm high and 10 mm wide in a diamond array with frontal area index 0.23; streamwise and vertical velocity components were measured with a special three-hot-wire anemometer designed for optimum performance in flows of high turbulence intensity. We found that:

(i) The momentum flux due to spatial correlations between time-averaged streamwise and vertical velocity components (the dispersive flux) was negligible, at heights near and above the top of the canopy.

(ii) In the turbulent energy budget, turbulent transport was a major loss (of about one-third of local production) near the top of the canopy, and was the principal gain mechanism lower down. Wake production was greater than shear production throughout the canopy. Pressure transport just above the canopy, inferred by difference, appeared to be a gain in approximate balance with the turbulent transport loss.

(iii) In the shear stress budget, wake production was negligible. The role of turbulent transport was equivalent to that in the turbulent energy budget, though smaller.

(iv) Velocity spectra above and within the canopy showed the dominance of large eddies occupying much of the boundary layer and moving downstream with a height-independent convection velocity. Within the canopy, much of the vertical but relatively little of the streamwise variance occurred at frequencies characteristic of wake turbulence.

(v) Quadrant analysis of the shear stress showed only a slight excess of sweeps over ejections near the top of the canopy, in contrast with previous studies. This is a result of improved measurement techniques; it suggests some reappraisal of inferences previously drawn from quadrant analysis.

1. Introduction

Over the last few years, it has been recognized that turbulence within and just above a plant canopy is dominated by quite coherent structures which (i) have vertical length scales at least as large as the canopy height, (ii) are intermittent and energetic, and (iii) account for most of the transport of momentum and scalar properties such as heat, water vapour and CO_2. The experimental evidence for this fairly recent development in our picture of canopy turbulence comes from observations of coherent waving ('honami') in cereal canopies (Finnigan, 1979a, b); from conditional analysis of turbulence data close to roughness arrays in the wind tunnel (Raupach, 1981) and plant canopies in the field (Shaw *et al.*, 1983); and from two-point velocity measurements above and within canopies (Seginer and Mulhearn, 1978). These large, coherent structures have been visualized principally as gusts, following the work of Finnigan (1979b).

[1] Present address: Head, Horticultural Engineering Division, National Institute of Agricultural Engineering, Wrest Park, Silsoe, Bedford MK45 4HS, U.K.

Boundary-Layer Meteorology **35** (1986) 21–52.

Such a picture has profound implications for theories of scalar transport or dispersion in the canopy environment. It has been realized for some time that simple gradient-diffusion theories for scalar and momentum transport are untenable because their basic requirement – that the length scale of the mixing process be substantially smaller than that of the inhomogeneity in the mean scalar or momentum gradient – is seriously violated (Corrsin, 1974). In the search for alternatives, attention has been directed to higher-order closure theories (Wilson and Shaw, 1977; Finnigan, 1985), or to random-flight theories in which the trajectories of dispersing tracer particles are represented by a Markov process in Lagrangian velocity space (e.g., Legg, 1983). However, from both the fundamental and practical viewpoints, these theories are still at an early stage of development.

This paper is the first of a series of three describing experiments on the dispersion of a passive scalar (trace heat) in a wind-tunnel model of a plant canopy. The overall aims of the work are to elucidate further the properties and dynamics of turbulence within and just above plant canopies, to give insight into how this turbulence disperses passive scalar additives, and to enable the developing theories mentioned above to be guided by good-quality data. This paper considers the aerodynamics of the model canopy – the wind field. The second paper (Coppin, Raupach and Legg, 1986, henceforth called II) treats dispersion from a horizontal plane source within the canopy, at a height of $0.80\,h_c$ (where h_c is the canopy height), while the third (Legg *et al.*, 1986, henceforth called III) considers dispersion from a lateral line source, at height $0.85\,h_c$.

Although the main motivation for this work was the scalar dispersion studies (II and III), the aerodynamic results were significant in several respects. Two new techniques were used: firstly, the data have been interpreted using the concept of spatial averaging, which not only smooths the spatial variability of the canopy but also incorporates directly all the dynamical effects of the canopy into the equations governing the averaged flow. Secondly, the velocity sensor was a three-hot-wire probe designed for measuring two velocity components in highly turbulent flows (Legg *et al.*, 1984), which permitted more reliable measurements of the turbulence within the canopy than had been possible in previous experiments using X-wires. Besides giving useful new or confirmatory data on dispersive fluxes, spectral dynamics and the budgets for turbulent energy and shear stress, these measurements indicate that X-wires are subject to errors within the canopy (especially for quadrant analysis of the shear stress) and that some reappraisal is necessary in this light.

2. Spatially Averaged Equations

To describe flow and transport in the plant canopy environment, we must use spatially averaged conservation equations for momentum and scalars for two main reasons: they incorporate naturally the surface influences which produce form and viscous drag and scalar sources and sinks, and they average the spatial variability imposed by plant parts. This averaging process is far more than a matter of statistical smoothing, as it introduces additional, physically significant terms accounting for dispersive fluxes and wake pro-

duction. Wilson and Shaw (1977) and Raupach and Shaw (1982) considered area averages over a horizontal plane intersecting numerous plants, while Finnigan (1985) generalized the area average to a volume average over any volume V within the canopy and gave volume-averaged equations for scalar conservation and transport. The two types of average are identical when V is an extensive, infinitesimally thin horizontal slab.

For later reference, we here give the volume-averaged form of the mean momentum equation. The volume average of any scalar or vector component $\phi(\mathbf{x}, t)$ is denoted by angle brackets and is defined as

$$\langle \phi \rangle(\mathbf{x}, t) = \frac{1}{V} \int\int\int_{V} \phi(\mathbf{x} + \mathbf{r}, t)\, \mathrm{d}\mathbf{r}\,, \tag{1}$$

where the averaging volume V excludes plant parts. Decomposing ϕ into its volume average and a departure therefrom (denoted by a double prime), we have

$$\phi = \langle \phi \rangle + \phi''\,, \tag{2}$$

where the departure $\phi''(\mathbf{x}, t)$ satisfies

$$\langle \phi'' \rangle = 0 \tag{3}$$

provided that the length scale of the spatial averaging in each coordinate direction is much less than the corresponding length scale of large-scale, nonrandom inhomogeneity. For a horizontally uniform canopy with systematic variation in the vertical direction only, this condition is met by making V a thin, horizontal slab.

The volume-averaging operator does not commute with spatial differentiation (or with temporal averaging if the plants are waving). Instead, Equation (1) implies that

$$\begin{aligned} \left\langle \frac{\partial \phi}{\partial x_i} \right\rangle &= \frac{\partial \langle \phi \rangle}{\partial x_i} - \frac{1}{V} \int\int_{S_I} \phi n_i \, \mathrm{d}S\,, \\ \left\langle \frac{\partial \phi}{\partial t} \right\rangle &= \frac{\partial \langle \phi \rangle}{\partial t} + \frac{1}{V} \int\int_{S_0 + S_I} \phi v_i n_i \, \mathrm{d}S\,, \end{aligned} \tag{4}$$

where S_0 is the outer or free part of the bounding surface S of V, S_I is the part of S which coincides with plant surfaces (so that $S = S_0 + S_I$), n_i is the unit normal vector pointing away from S into V and v_i is the velocity of the surface S. If these plants are waving or fluttering, v_i will be nonzero over S_I; however, v_i is zero over S_0, since the whole averaging volume does not move.

We next apply the volume-averaging operator to the continuity equation and the Reynolds equation for mean momentum conservation at a single point. For a flow without buoyancy forces, these equations are (employing the tensor summation convention)

$$\frac{\partial u_i}{\partial x_i} = \frac{\partial \overline{u}_i}{\partial x_i} = \frac{\partial u_i'}{\partial x_i} = 0 \tag{5}$$

and

$$\frac{\partial \overline{u}_i}{\partial t} + \overline{u}_j \frac{\partial \overline{u}_i}{\partial x_j} = -\frac{\partial \overline{u_i' u_j'}}{\partial x_j} - \frac{\partial \overline{p}}{\partial x_i} + \nu \nabla^2 \overline{u}_i , \tag{6}$$

where u_i and x_i are velocity and position vectors, t time, p the kinematic pressure and ν the kinematic viscosity; overbars and single primes denote, respectively, single-point time averages and departures therefrom. Volume averaging gives

$$\frac{\partial \langle \overline{u}_i \rangle}{\partial x_i} = 0 \tag{7}$$

and

$$\frac{\partial \langle \overline{u}_i \rangle}{\partial t} + \langle \overline{u}_j \rangle \frac{\partial \langle \overline{u}_i \rangle}{\partial x_j} = -\frac{\partial \langle \overline{p} \rangle}{\partial x_i} + \frac{\partial \tau_{ij}}{\partial x_j} + f_{Fi} + f_{Vi} \tag{8}$$

with

$$\tau_{ij} = -\langle \overline{u_i' u_j'} \rangle - \langle \overline{u}_i'' \overline{u}_j'' \rangle + \nu \frac{\partial \langle \overline{u}_i \rangle}{\partial x_j} , \tag{9}$$

$$f_{Fi} = \frac{1}{V} \int\int_{S_I} \overline{p} n_i \, \mathrm{d}S , \tag{10}$$

$$f_{Vi} = -\frac{\nu}{V} \int\int_{S_I} \frac{\partial \overline{u}_i}{\partial n} \, \mathrm{d}S . \tag{11}$$

Here f_{Fi} and f_{Vi} are the form and viscous drag force vectors exerted on a unit mass of air within the averaging volume, τ_{ij} is the volume-averaged kinematic momentum flux or stress tensor, and $\partial/\partial n$ denotes differentiation along n_j. Equation (9) shows that τ_{ij} includes not only the conventional turbulent and molecular stresses (the first and last terms, respectively), but also a dispersive stress (the middle term) due to spatial correlation within V of time-averaged but position-dependent quantities (Wilson and Shaw, 1977). These volume-averaged equations do not contain v_i, and so are true for both rigid and waving canopies.

From now on we shall use meteorological rather than tensor notation, writing $x_i = (x, y, z)$ and $u_i = (u, v, w)$ with the x-coordinate in the mean streamwise direction and the z-coordinate normal to the ground. The averaging volume V will be regarded as a thin horizontal slab of variable height z; since we are considering a regular model

canopy, it is sufficient for V to encompass only one 'unit cell' of the canopy on the xy plane. To an excellent approximation, spatially averaged flow properties within our canopy (except very close to its leading edge) are functions of z only, as shown later; also, the mean streamwise pressure gradient is zero and the flow is stationary. With these constraints, the streamwise component of Equation (8) becomes

$$\frac{\partial}{\partial z}\left(\langle \overline{u'w'} \rangle + \langle \overline{u}''\overline{w}'' \rangle - \nu \frac{\partial \overline{u}}{\partial z}\right) = f_x , \tag{12}$$

where f_x $(= f_{F1} + f_{V1})$ is the total streamwise drag per unit mass of air within the averaging volume. When form drag is the principal drag mechanism, a suitable parameterization for f_x is

$$f_x = -\tfrac{1}{2} C_D a \langle \overline{u} \rangle^2 , \tag{13}$$

where C_D is an element drag coefficient and a is the element area density (frontal area per unit volume). Because C_D is an *in situ* drag coefficient, it must account for the effects upon the drag of canopy turbulence, through both intensity and length scale, and also of 'sheltering' within the canopy.

3. Experimental Arrangement and Technique

3.1. The wind tunnel and model canopy

The experiments were done in the CSIRO Pye Laboratory wind tunnel, an open-return blower tunnel with a 5.5 : 1 two-dimensional contraction and a working section 10.6 m long, 1.78 m wide, and 0.65 m high (Wooding, 1968). The tunnel arrangement is shown in Figure 1. A 50 mm fence tripped the flow entering the working section, generating a deep turbulent boundary layer that was developed initially over a section of roughness constructed from 15 mm stones (Mulhearn and Finnigan, 1978). The stony surface was raised (see Figure 1) so that its zero-plane displacement matched that estimated *a priori* for the canopy (48 mm). The flow then encountered the model canopy, which extended

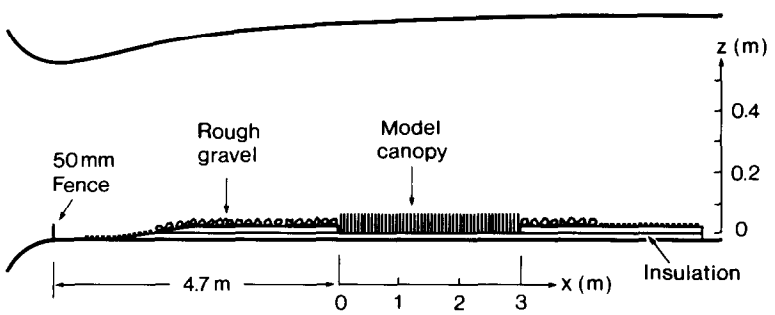

Fig. 1. The experimental arrangement. Note exaggerated vertical scale.

for 3.0 m in the streamwise direction and covered the full width of the tunnel. The canopy was an array of vertical aluminium strips, each 10 mm wide, 1 mm thick, and 60 mm tall, arranged in a regular diamond pattern with 60 mm cross-stream and 44 mm streamwise spacing, as shown in Figure 2. Downstream of the canopy, the flow encountered a similar raised stony surface to that used for initial flow development. Because heat was the tracer for the dispersion experiments, the whole floor beneath the working section was insulated with a sheet of polystyrene foam, 25 mm thick. The flexible roof of the working section was adjusted to give zero streamwise pressure gradient over the canopy. The coordinate origins were the leading edge of the canopy ($x = 0$) and the ground surface beneath the canopy elements ($z = 0$). For later reference, the main physical and aerodynamic parameters are summarized in Table I.

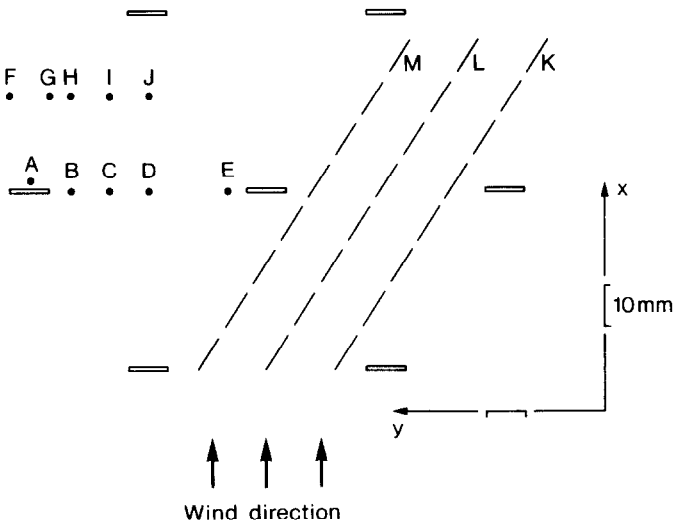

Fig. 2. View from above of the arrangement of roughness elements, showing locations for three-wire probe traverses (A to J) and sonic traverses (K to M).

TABLE I

Summary of physical and aerodynamic parameters

Canopy height	h_c	60 mm
Frontal area index	λ	0.23
Boundary-layer depth	δ	540 mm
Free-stream velocity	U_∞	11.25 m s^{-1}
Mean velocity at h_c	$\langle \overline{u} \rangle (h_c)$	3.40 m s^{-1}
Friction velocity	u_*	1.03 m s^{-1}
Roughness length	z_0	8.7 mm
Zero-plane displacement	d	43 mm
Reynolds numbers:		
boundary-layer	$U_\infty \delta / \nu$	4.0×10^5
roughness	$u_* z_0 / \nu$	600

3.2. VELOCITY MEASUREMENTS

The u and w components of the velocity vector were measured with the three-hot-wire anemometer described by Legg *et al.* (1984), which consists of a standard, vertically-oriented X-wire probe with an additional vertical wire adjacent to it. Each hot-wire was 1 mm long, and the lateral distance between the outermost wires was 2.5 mm. The three-wire probe was specifically designed to yield maximum information in the highly turbulent flow just above and within the model canopy. In contrast to the conventional X-probe, which has an acceptance angle of less than $\pm 45°$ and gives reasonable accuracy only in turbulence intensities ($i_u = \sigma_u/\bar{u}$) of less than 0.3, the three-wire probe has an acceptance angle close to $\pm 90°$ and performs satisfactorily when i_u is 0.5 or higher. As the velocity data were measured in conjunction with the heat dispersion experiments (II and III), the full sensor assembly consisted of the three-wire probe for measuring u and w and a cold-wire thermometer for measuring the temperature θ.

The three-wire probe in this application is subject to errors of several kinds, including (a) error at high turbulence intensities due to short-term flow reversals in the streamwise direction; (b) error due to contamination of the (u, w) velocity vector by lateral (v-component) velocity fluctuations; (c) the effect of heat dispersed from one hot-wire on the readings of another; (d) the effect of fluctuating air temperatures upon the hot-wires; and (e) the loss of high-frequency coherence due to the spatial separation of the wires. Errors (a) and (b) were estimated theoretically by Legg *et al.* (1984); however, we have not applied their error estimates as corrections to any of the data in this paper, or in II or III. Our results for $\overline{u'w'}$ suggest that the errors estimated by Legg *et al.* (1984) may be too large (see Section 5). Error (c) was insignificant (as shown by examining signals from individual hot-wires with and without the other hot-wires turned on) while (d) was a small error which was corrected for during data processing. Error (e) is probably not serious for velocity, as the maximum wire separation in the three-wire probe (2.5 mm) is substantially less than either the canopy depth (60 mm) or the width of the canopy elements (10 mm), which control the length scales of the shear and wake turbulence, respectively, within the canopy.

Vertical traverses, each consisting of 20 levels between $z = 5$ mm and $z = 380$ mm, were made with the sensor assembly at stations between $x = 0.44$ m and $x = 2.47$ m. All signals were low-pass filtered at 1 kHz (Butterworth, 96 dB/octave), digitized on-line at 2 kHz and recorded on magnetic tape continuously for 20 s at each measurement position. The velocity data were processed by first applying a nonlinear wind calibration to obtain instantaneous effective cooling velocities for the three wires, accounting for error (d) as in Raupach and Legg (1983). Then the cooling velocities were converted to time series for u and w by method 1 of Legg *et al.* (1984), which takes approximate account of v-component velocity fluctuations. From these time series, all moments of u and w up to third order were calculated.

Because turbulence intensities within and just above the canopy were very high ($i_u \approx 0.6$), supplementary measurements of mean streamwise velocity in the region $z < 100$ mm were made with a miniature one-component sonic anemometer with a path

length of 100 mm (an early version of the instrument of Coppin and Taylor, 1983). The sonic gives a line average of the velocity component along the sound path, and suffers from none of the three-wire probe errors (a) to (e).

Vertical and streamwise gradients of measured moments, required for the calculation of turbulent diffusivities and budgets, were calculated at each x-station from measurements at positions C and D (see Figure 2). Sliding polynomials (e.g., 5 point, third degree) were fitted to each vertical profile of each moment, enabling fitted values and vertical derivatives to be read at 35 preset heights between 5 and 250 mm. Results from the profiles at positions C and D were then averaged, giving values that were taken to represent horizontal averages within a canopy cell; this assumption is justified in the next section. For $\langle \bar{u} \rangle$ and $\partial \langle \bar{u} \rangle / \partial z$ below $z = 70$ mm, sonic data rather than three-wire probe data were used. Finally, averaged vertical profiles at all x-stations were combined to calculate streamwise derivatives.

4. Local Heterogeneity in the Wind Field

4.1. Mean wind field and dispersive momentum flux

For our model canopy with its large bluff elements, local heterogeneity is very severe because of the presence of separation zones to the front and rear of each element. A survey of the local wind pattern (with the restriction that measurements were impossible very close to the elements) was undertaken only at $x = 1.25$ m. However, we show later that there was negligible streamwise evolution of the wind pattern within the canopy for $x > 0.5$ m, so the results given in this section apply everywhere except very close to the leading edge of the canopy.

Figure 3(a) shows three-wire profiles of $\bar{u}(z)$ at 10 positions (A to J in Figure 2) within a canopy cell at $x = 1.25$ m. The sonic data for $\bar{u}(z)$, shown in Figure 3(b), are line averages of $\bar{u}$ over 100 mm diagonal paths (K, L, and M in Figure 2), also at $x = 1.25$ m.

Both types of data illustrate the strong horizontal heterogeneity of the flow within the canopy, with profiles measured in element wakes (A, F, G, and K) giving substantially lower $\bar{u}$ values than the horizontal average.

Figure 3(c) shows the horizontally-averaged* mean wind profile $\langle \bar{u} \rangle(z)$ from the sonic and three-wire probe. In the lower half of the canopy, $\langle \bar{u} \rangle$ from the three-wire probe is significantly higher than that from the sonic. Because of the flow reversal problems associated with the three-wire probe, we regard the sonic profile as the more reliable measurement within the canopy and therefore use it in subsequent analysis, as already outlined. However, Figure 3(b) shows that the uncertainty in $\langle \bar{u} \rangle$ from the sonic is about ± 0.25 m s^{-1} from the horizontal variability alone.

* For the three-wire probe, the average was $(A + B + 2C + D + E + (F + G)/2 + 2H + 2I + J)/12$, (obtained by partitioning a canopy cell, in the xy plane, into regions represented by the various profiles, and then weighting each profile by the fraction of the total area that it represents). The sonic average was weighted as $(2.5K + 1.75(L + M))/6$ to account for the fact that no sonic data could be obtained from the diagonal path through the elements themselves, which should more closely resemble K than L or M.

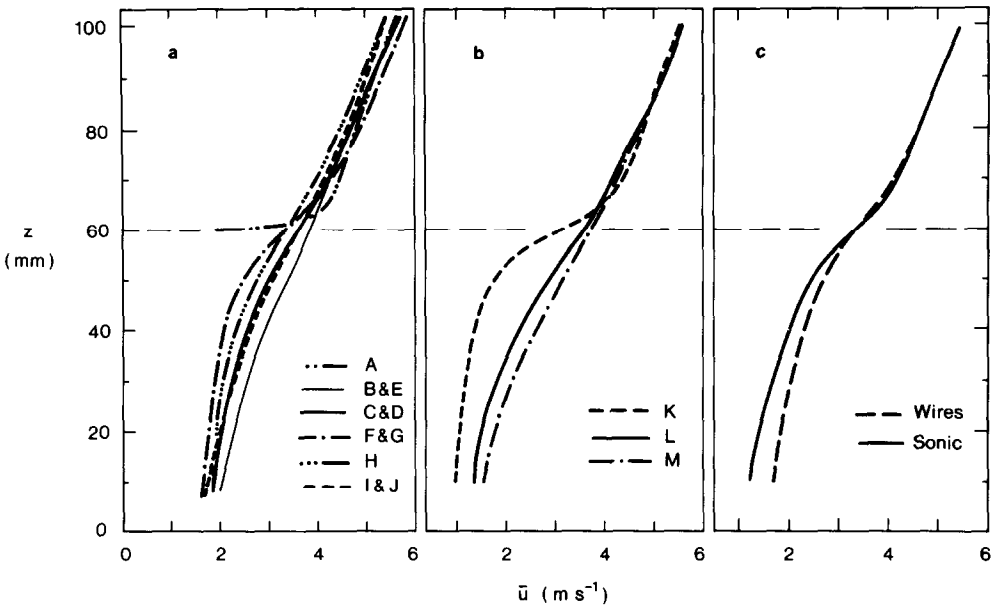

Fig. 3. (a) three-wire profiles of $\bar{u}(z)$; (b) sonic profiles of $\bar{u}(z)$; (c) profiles of $\langle \bar{u} \rangle(z)$ from the sonic and the three-wire probe. All measurements made within a canopy cell at $x = 1.25$ m. In (a), symmetrically placed positions are represented by a single line. Positions C and D, although not symmetric, differ insignificantly and are shown by only one line.

The systematic nature of the mean wind field variation across a canopy cell is better illustrated in Figure 4, where contours of equal $\bar{u}$ and $\bar{w}$ are shown at $z = 62$ mm, just above the top of the canopy. The $\bar{u}$ contours show the wake region and a meandering high-speed jet of air snaking between the elements. The $\bar{w}$ contours are superimposed upon an apparent horizontal average, $\langle \bar{w} \rangle$, of about -0.15 m s^{-1}, which is approximately consistent with the estimate of Legg *et al.* (1984) for the apparent $\bar{w}$ induced by three-wire probe errors. We can confidently attribute the measured $\langle \bar{w} \rangle$ to probe error because continuity requires that $\langle \bar{w} \rangle(z) = 0$ in the absence of streamwise development of the flow beneath z. If the measured $\langle \bar{w} \rangle$ is removed from Figure 4(b) as an offset error which is everywhere constant, then a pattern emerges of local updraught just in front of each canopy element, with a roughly equal and opposite strength and area of local downdraught some distance behind each element. The maximum streamline slopes in these updraught and downdaught regions are about $\pm 4°$.

From Figure 4 we can calculate the dispersive momentum fluw $\langle \bar{u}'' \bar{w}'' \rangle$: at $z = 62$ mm, $\langle \bar{u}'' \bar{w}'' \rangle$ is about -0.01 m^2 s^{-2}, whereas $\langle \overline{u'w'} \rangle$ is -1.06 m^2 s^{-2} (see later). Thus, the dispersive momentum flux at this height is negligible compared to the turbulent flux. Unfortunately, this finding cannot be extended reliably to heights within the canopy because of the inability to measure very close to the elements and also because of the three-wire probe errors induced by high turbulence intensities. However, dispersive fluxes appear to remain small at least in the upper part of the canopy; for

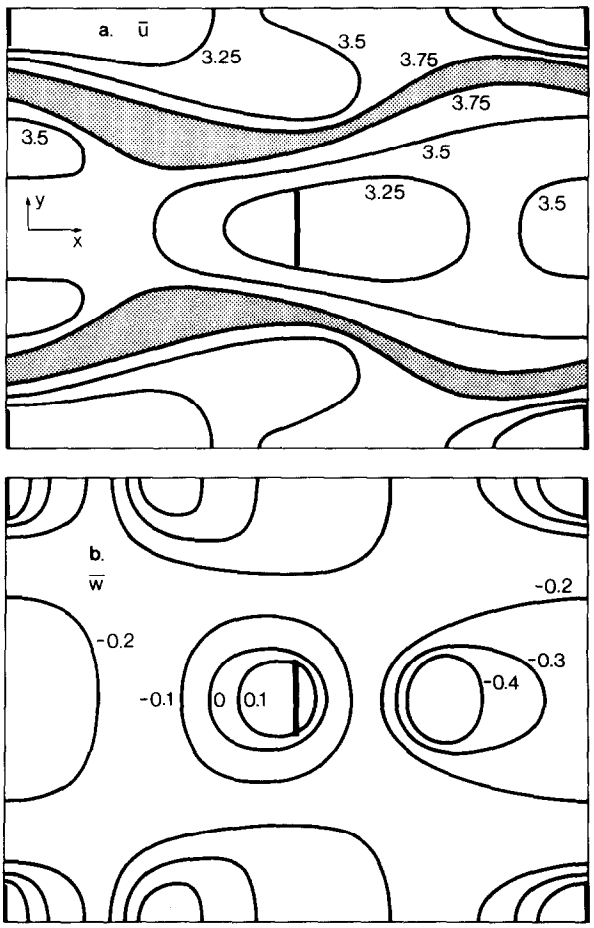

Fig. 4. Contours of (a) $\bar{u}$, (b) $\bar{w}$ at $z = 62$ mm, for a canopy cell at $x = 1.25$ m. Shaded region in (a) represents the meandering high-speed jet.

example, at $z = 40$ mm, we estimate $\langle \bar{u}''\bar{w}'' \rangle$ to be 0.05 of $\langle \overline{u'w'} \rangle$. The firm conclusion is that dispersive momentum fluxes are insignificant for $z \gtrsim h_c$. This agrees with earlier findings from more limited data (Mulhearn, 1978; Raupach *et al.*, 1980).

4.2. Turbulent wind field

Figure 5(a) shows vertical profiles of $\overline{u'w'}$ at the same positions relative to the canopy elements as in Figure 3(a). The scatter in $\overline{u'w'}$ within the canopy is very large, with $|\overline{u'w'}|$ being least behind an element (position *F*, *G*, and *H*). Measured $\overline{u'w'}$ values are positive in the lowest quarter or so of the canopy. Because of the high three-wire probe errors in this region, it is not possible to interpret the positive $\overline{u'w'}$ values with confidence. However, if real, they may be associated with systematic recirculations in element wakes, and hence with significant dispersive fluxes, in the lower canopy. There

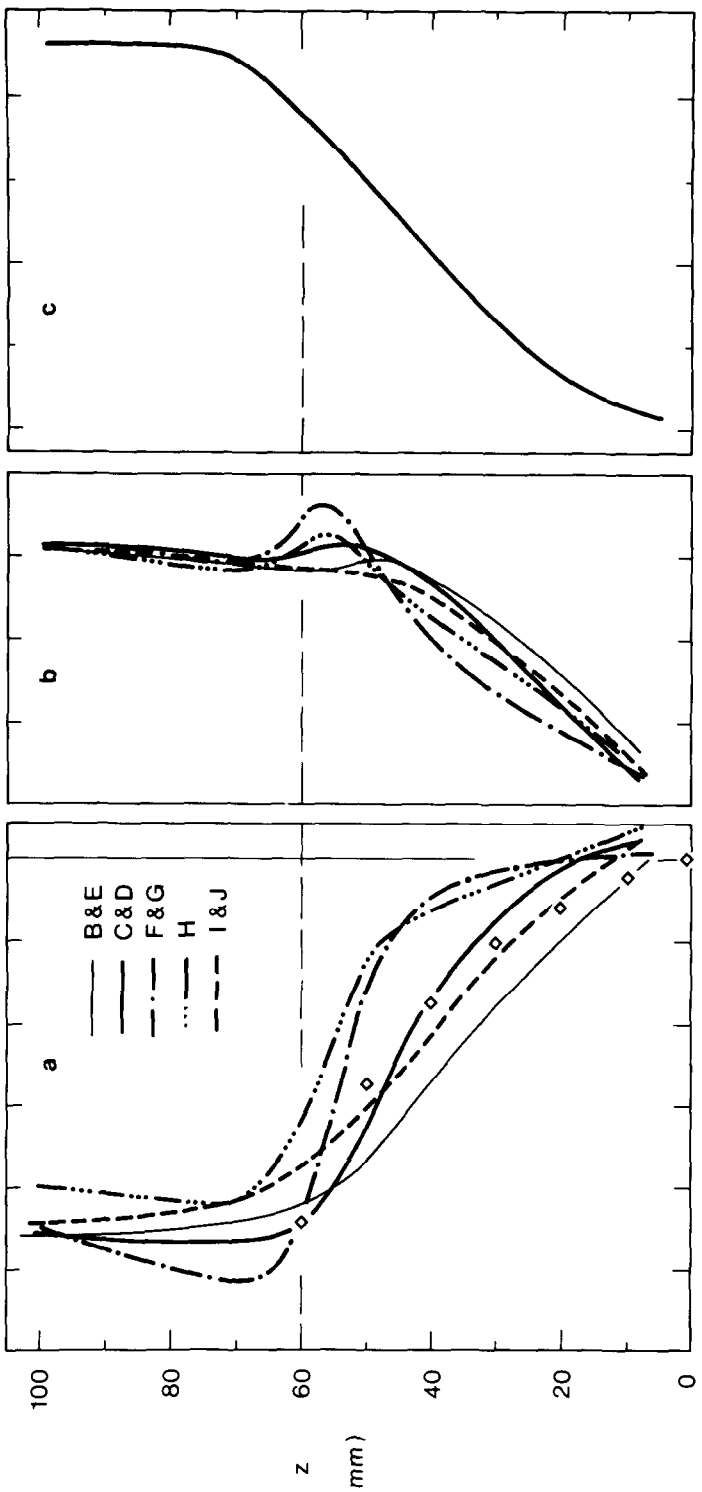

Fig. 5. Vertical profiles of (a) $\overline{u'w'}$, (b) σ_w, (c) σ_u within a canopy cell at $x = 1.25$ m. Points in (a) denote $\langle \overline{u'w'} \rangle$ profile from Equations (12) and (13) with C_D = constant.

is evidence for such recirculations from the behaviour of the mean plume height from a lateral line source (see III).

For comparison, Figure 5(a) also shows a $\langle \overline{u'w'} \rangle$ profile derived by integrating Equations (12) and (13) with the assumptions that C_D is independent of height in the canopy, that dispersive and molecular contributions to the momentum flux are negligible and that $\langle \overline{u'w'} \rangle = 0$ at $z = 0$ (in other words, that the momentum absorbed by the ground is negligible compared with that absorbed by the elements). The value of C_D was set so that $\langle \overline{u'w'} \rangle$ at h_c, when calculated by this method, matched the three-wire measurement; this gave $C_D = 1.6$. The $\langle \overline{u'w'} \rangle$ profile from Equations (12) and (13) falls well within the wide scatter of the measured $\overline{u'w'}$ profiles in Figure 5(a).

The value $C_D = 1.6$ is rather high but not implausible. The drag coefficient of a rectangular plate, normally exposed to a uniform stream, varies from 1.18 to 2 as the aspect ratio increases from 1 to infinity (Hoerner, 1965). The turbulent environment within the canopy, however, means that the free-stream drag coefficient is of little relevance (Finnigan and Raupach, 1986).

The σ_w profiles within the canopy (Figure 5(b)) show pronounced local maxima near $z = h_c$ and just behind an element, where significant longitudinal vorticity generation occurs in the element's wake. Not surprisingly, no such local maxima are evident in the σ_u profiles (Figure 5(c)). The σ_u profiles do not vary systematically among positions *B* to *J* within the canopy, and are represented by a single line. The turbulence intensities $\sigma_w/\overline{u}$ and $\sigma_u/\overline{u}$ do not vary strongly either with height or with position (*B* to *J*), taking values of about 0.38 and 0.55, respectively. These are substantially lower than the values reported by Wilson *et al.* (1982) for a corn canopy in the field; those authors found that $\sigma_w/\overline{u}$ was between 0.5 and 2 and $\sigma_u/\overline{u}$ between 1 and 4, the highest values occurring low in the canopy.

The data in Figure 3 and 5 confirm that profiles at positions *C* and *D* are representative of horizontally averaged profiles within a canopy cell. Measurements at these positions only were used in the work reported from here on.

5. Large-Scale Properties of the Turbulent Wind Flow

5.1. Overall streamwise development

The overall streamwise development of the boundary layer above and within the model canopy is shown in Figure 6 by profiles of $\overline{u}$, σ_u, σ_w and $\overline{u'w'}$ at five *x*-stations between $x = 0.44$ and $x = 2.47$ m. All profiles were measured at position *D* in Figure 2. The height axis has not been normalized because the flows in the outer boundary layer and within the canopy require different normalizing length scales.

The flow above the canopy is developing as one would expect of a smooth-to-rough transition. Thus , $\overline{u'w'}$, σ_u and σ_w all decrease strongly with height at $x = 0.44$ m, but are approximately independent of height (up to at least $z = 120$ mm) at $x = 2.47$ m, indicating the development of an equilibrium surface layer over the model canopy.

Within the canopy there is negligible development with x except for σ_u upstream of $x = 1$ m.

We now examine in detail the second and third moments of u and w, deferring a consideration of the mean wind $\bar{u}$ to the next section.

5.2. Shear stress and friction velocity

At $x = 2.47$ m, a layer of approximately constant shear stress, $\overline{u'w'}$, has been established between h_c and $2\,h_c$ ($z = 60$ to 120 mm). The total kinematic drag on the canopy defines the friction velocity u_*, since

$$u_*^2 = \left(- \langle \overline{u'w'} \rangle - \langle \bar{u}''\bar{w}'' \rangle + \nu \frac{\partial \langle \bar{u} \rangle}{\partial z} \right)_{z = h_c} \tag{14}$$

in the absence of streamwise development within the canopy. However, the dispersive and molecular flux terms are negligible; also, for $z \geq h_c$ there is no significant difference between $\langle \overline{u'w'} \rangle$ and $\overline{u'w'}$ at position D (see Figure 5). Hence u_*^2 is given to a close approximation by the $\overline{u'w'}$ values from the constant-stress layer evident in Figure 6. Determinations at x-stations between 0.44 and 2.47 m give $u_*^2 = 1.06\ \mathrm{m^2\ s^{-2}}$, with negligible dependence on x.

An independent value for u_*^2 can be obtained from the integral momentum balance equation for an adiabatic turbulent boundary layer with zero pressure gradient (Rouse, 1959, p. 317):

$$u_*^2 = U_\infty^2 \left(\frac{\mathrm{d}\theta}{\mathrm{d}x} + \frac{\mathrm{d}I}{\mathrm{d}x} \right), \tag{15}$$

where U_∞ is the free stream velocity, θ the momentum thickness

$$\theta = \int_0^\infty \frac{\bar{u}}{U_\infty} \left(1 - \frac{\bar{u}}{U_\infty} \right) \mathrm{d}z \tag{16}$$

and I the integral

$$I = \frac{1}{U_\infty^2} \int_0^\infty (\overline{w'^2} - \overline{u'^2}) \mathrm{d}z\,. \tag{17}$$

Table II shows $\theta(x)$ and $I(x)$ at several x-stations; with the integral momentum equation, these data give $u_*^2 = 1.00 \pm 0.1\ \mathrm{m^2\ s^{-2}}$, so both methods for finding u_*^2 agree to within experimental error. Henceforth, we use the value from the three-wire measurements. This comparison provides support for the uncorrected three-wire measurements of u and w in the region $z \geq h_c$, and also suggests that the three-wire probe errors estimated by Legg *et al.* (1984) are too large. Their calculations imply a measured $|\overline{u'w'}|$ at $z = h_c$ of only 70% of the true value, which is not supported by the direct comparison.

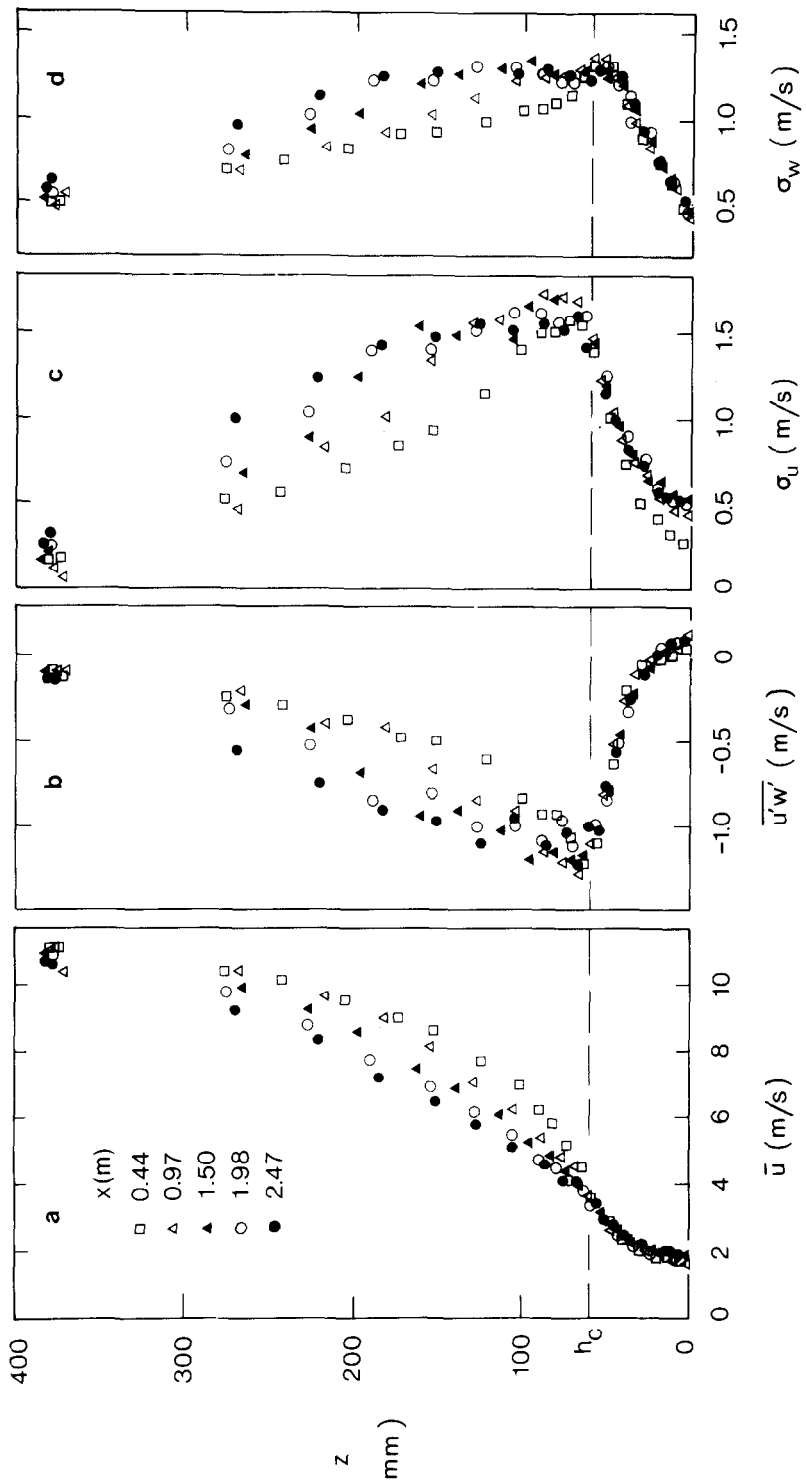

Fig. 6. Profiles of (a) $\bar{u}$, (b) $\overline{u'w'}$, (c) σ_u, (d) σ_w at five x-stations. All data measured with three-wire probe at position D within a canopy cell.

TABLE II

Components of the integral momentum balance

x (m)	θ (mm)	I (mm)
0.44	48.5	−3.2
1.50	57.4	−4.5
2.47	66.0	−4.8

5.3. STANDARD DEVIATIONS OF u AND w

The standard deviations σ_u and σ_w (Figure 6) are approximately independent of height in the constant-stress region above the canopy. In this region the ratios σ_u/u_* and σ_w/u_* are 2.06 and 1.21, respectively, both slightly lower than the widely-used typical values $\sigma_u/u_* \approx 2.5$ and $\sigma_w/u_* \approx 1.25$ in the near-neutral atmospheric surface layer (e.g., Panofsky, 1974). The fact that σ_u/u_*, in particular, is rather low suggests that our boundary layer does not have as much large-scale 'inactive motion' (Bradshaw, 1967) as the atmospheric surface layer or typical laboratory boundary layers which simulate it (Fackrell and Robins, 1982; Raupach and Legg, 1983). This is probably so because, in the present experiment, the length scales associated with the canopy were not sufficiently small compared with the total boundary-layer depth δ; for example, the ratio h_c/δ was 0.11. In contrast, for the gravel-roughness boundary layer of Raupach and Legg (1983), h_c/δ was 0.013, and in the atmosphere, h_c/δ is of order 10^{-3}.

5.4. HIGHER VELOCITY MOMENTS

The velocity third moments in skewness form (e.g. $Sk_{uuw} = \overline{u'u'w'}/(\sigma_u^2\sigma_w)$) are shown in Figure 7. For the region above the canopy, comparable data have been presented by Seginer *et al.* (1976), Mulhearn and Finnigan (1978), Raupach (1981) and Andreopoulos and Bradshaw (1981) for laboratory flows, and Maitani (1979) for the near neutral atmospheric surface layer. These data agree with ours in the following broad respect: the skewnesses all cross zero somewhere just above the canopy, subsequently increasing in magnitude with further increase in height, and alternating in sign (i.e., an even power of u makes the skewness positive) so that

$$Sk_{uuu} \approx -2\,Sk_{uuw} \approx 2\,Sk_{uww} \approx -1.5\,Sk_{www}\,.$$

These numerical ratios, from the data above the zero-crossing height in Figure 7, are close to those found by Raupach (1981) over several cylinder-roughened surfaces with different roughness densities. Maitani's (1979) summary of skewness measurements in the near-neutral atmospheric surface layer reveals no systematic departures from zero at heights up to 22 m, suggesting that the increasing magnitude of the skewnesses with height, as observed in laboratory boundary layers, is an essentially outer-layer effect.

The situation within the canopy is not so simple. Our data, like that of Seginer *et al.* (1976), Maitani (1979) and Raupach (1981), show that the skewnesses there alternate in sign as in the outer layer, but in the opposite sense (so that an odd power u makes

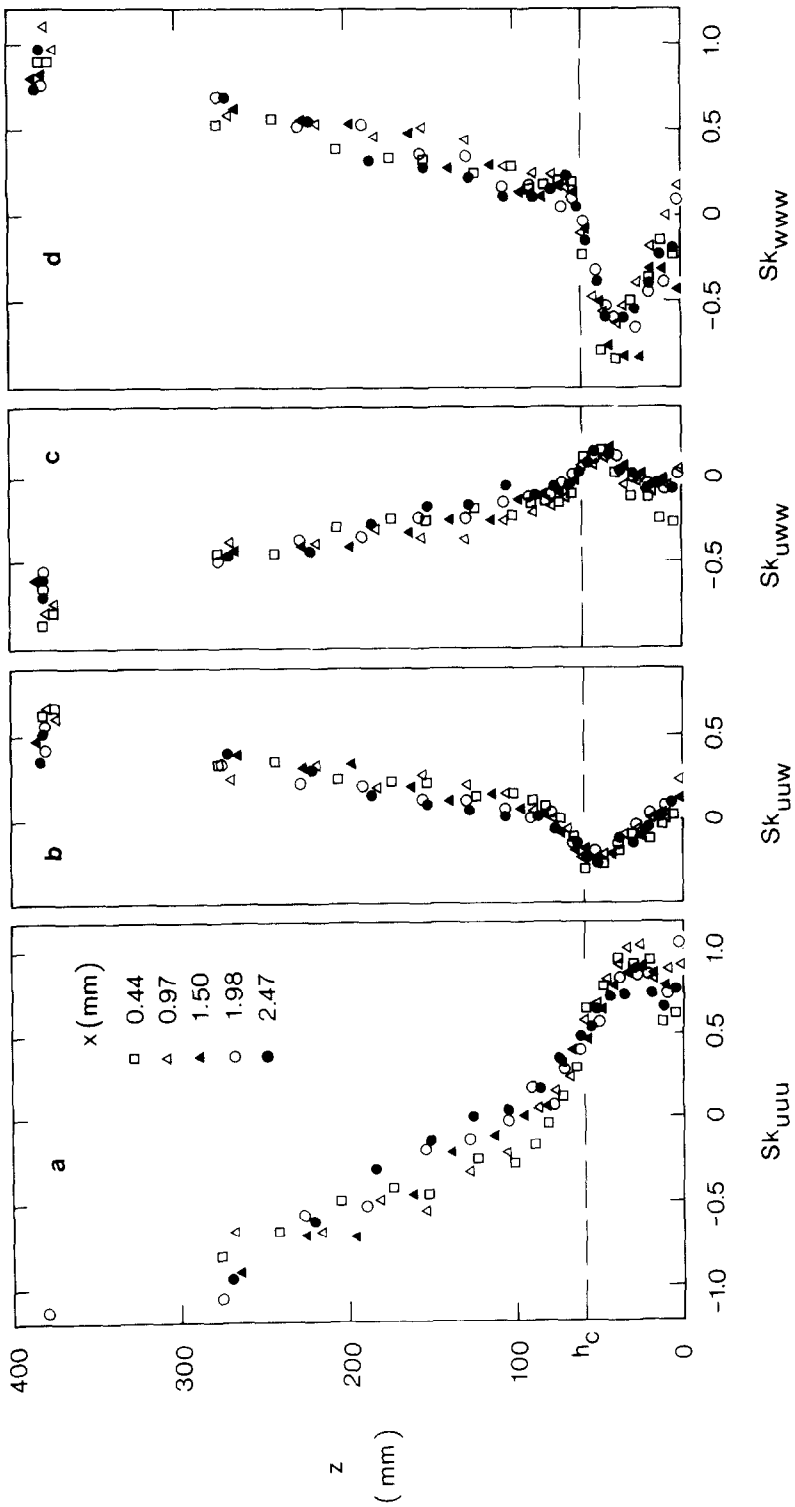

Fig. 7. Profiles of (a) Sk_{uuu}, (b) Sk_{uuw}, (c) Sk_{uww}, (d) Sk_{www}, at five x-stations. Details as in Figure 6.

the skewness positive). However, we find that the ratios between skewnesses are different to those in the outer layer and change considerably with height. At $z = 0.7\ h_c$, for example, we have

$$Sk_{uuu} \approx -4\ Sk_{uuw} \approx 5\ Sk_{uww} \approx -1.5\ Sk_{www},$$

the striking aspect of which is the relative smallness of the 'mixed' skewnesses Sk_{uuw} and Sk_{uww}. The 'pure' skewnesses for u and w are both large within the canopy, respectively reaching maximum magnitudes of $+1.0$ and -0.8; these high values provide evidence for the existence in our canopy of the intermittent, energetic, downward-moving gusts of the kind that Finnigan (1979b) found to be dominant in momentum transfer to waving wheat. As the canopy floor is approached, the u skewness remains large and positive but the w skewness approaches zero, probably because the solid boundary deflects downward-moving gusts into horizontal motions resembling transient wall jets. Our skewness profiles for u and w within the canopy agree well with the only other known detailed measurements within a model canopy, those of Seginer *et al.* (1976).

Figure 8 shows the kurtoses K_u and K_w for u and w. Just above the canopy, both $K_u(\approx 2.5)$ and $K_w(\approx 3.5)$ are fairly close to the Gaussian value of 3; both increase with z above the canopy in accord with known behaviour in equilibrium, zero-pressure-gradient boundary layers (Raupach, 1981). Within the canopy, K_u remains less than 4

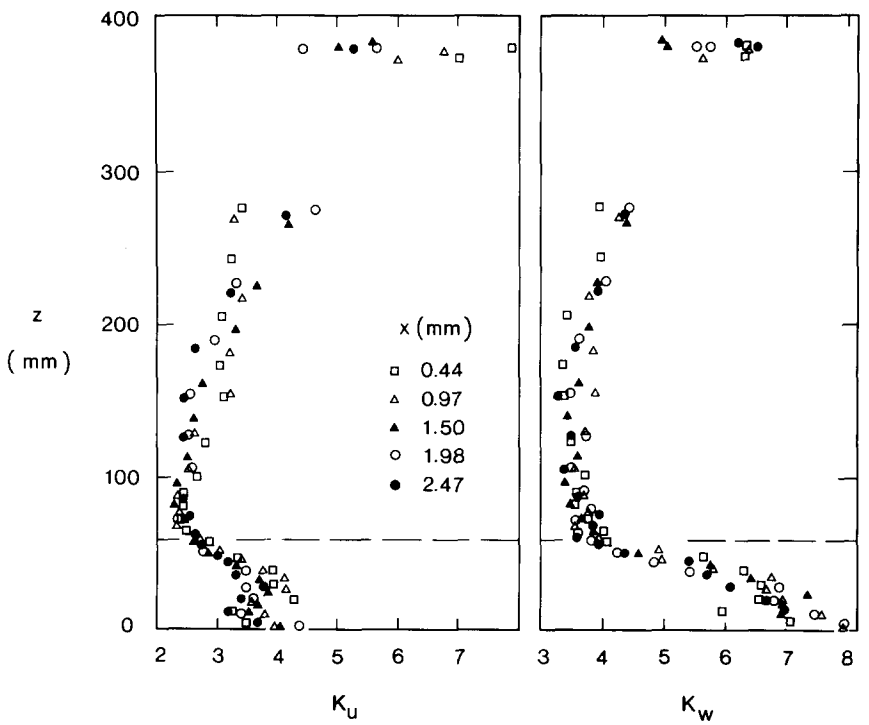

Fig. 8. Kurtoses (a) K_u and (b) K_w at five x-stations. Details as in Figure 6.

or so but K_w reaches quite high values, up to 7 or more. Hence, w is subject to extreme events with significantly greater than Gaussian probability, as well as being negatively skewed.

6. Mean Wind Field and Associated Parameters

6.1. Logarithmic wind profile

Figure 9 shows $\langle \bar{u} \rangle(z)$ plotted against $\ln(z - d)$ at five x-stations. The zero-plane displacement d was determined by the centre-of-pressure theorem (Thom, 1971; Jackson, 1981), which can be written

$$d = \left(\int_0^{h_c} z f_x(z)\, \mathrm{d}z \right) \Big/ \left(\int_0^{h_c} f_x(z)\, \mathrm{d}z \right). \tag{18}$$

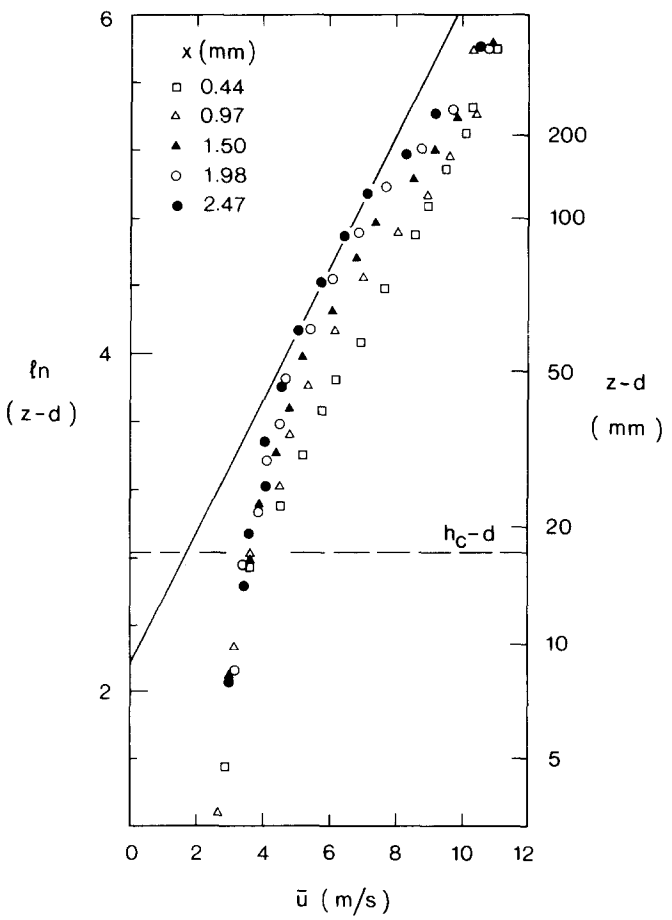

Fig. 9. Logarithmically plotted mean wind profile at five x-stations. Details as in Figure 6.

Equation (13) was used to find f_x by assuming C_D and a to be independent of height; they then disappear from Equation (18), leaving an expression for d in terms of $\langle \bar{u} \rangle(z)$. The sonic profile for $\langle \bar{u} \rangle$ gives $d = 43$ mm or $d/h = 0.72$.

The logarithmic law

$$\langle \bar{u} \rangle(z) = \frac{u_*}{k} \ln\left(\frac{z - d}{z_0}\right) \tag{19}$$

(where $k(= 0.40)$ is the von Karman constant and z_0 the roughness length) is shown in Figure 9 as a straight line drawn using the independently measured value of u_* (1.03 m s^{-1}). The line has been made tangential to the $\langle \bar{u} \rangle$ profile at the farthest downstream x-station ($x = 2.47$ m), where the boundary layer over the canopy is most developed. In fact, the measured $\langle \bar{u} \rangle$ profile obeys the logarithmic law only in a very limited inertial sublayer, bounded above by a conventional outer layer and below by a well-defined 'roughness sublayer'. In this sublayer, the profile slope $\partial \langle \bar{u} \rangle / \partial z$ is substantially less than the logarithmic law prediction, as observed also by Raupach *et al.* (1980) close to several cylinder-roughened surfaces of varying density. From the limited inertial sublayer at $x = 2.47$ m, we obtain $z_0 = 8.7$ mm or $z_0/h_c = 0.14$. This is a high but not implausible roughness length which, together with the roughness concentration $\lambda = 0.23$, places the model canopy at the peak of the z_0/h_c versus λ curve given by Raupach *et al.* (1980).

6.2. Eddy diffusivity for momentum

Figure 10 shows the experimentally derived eddy diffusivity for momentum, defined by

$$\langle \overline{u'w'} \rangle = -K_M \, \partial \langle \bar{u} \rangle / \partial z \, . \tag{20}$$

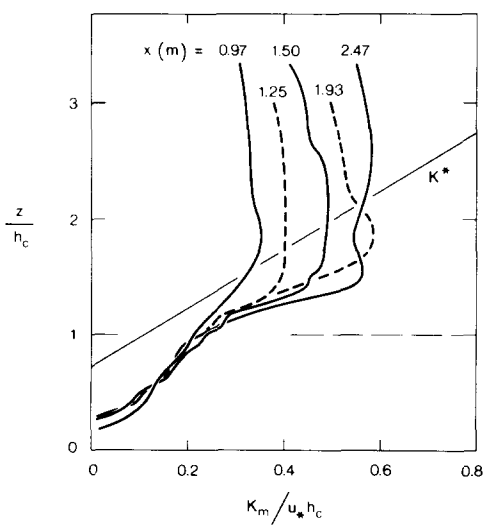

Fig. 10. Momentum eddy diffusivity K_M at five x-stations. Straight line represents the inertial-sublayer diffusivity $K^* = ku_* (z - d)$.

The roughness sublayer is clearly evident as a region between $z = h_c$ and $z \approx 1.5\,h_c$ where K_M is enhanced above its inertial-sublayer value, $K^* = ku_*(z - d)$. At $z = h_c$, $K_M = 2.0\,K^*$. With increasing x, a self-preserving profile for K_M (and for $\langle \bar{u} \rangle$, from Figure 9) develops from the surface upwards, so that the roughness sublayer becomes self-preserving before the inertial sublayer. Figure 10 also shows that in this experiment the inertial sublayer is 'squeezed out' between the roughness sublayer and an outer layer in which K_M is independent of z. This is another consequence of the high value of h_c/δ compared with the atmosphere and most other laboratory rough-wall boundary layer flows.

7. Spectra and Length Scales for u and w

Spectra show the behaviour of the time and length scales of the turbulence and also enable the dissipation rate for turbulent energy to be estimated. Figure 11 shows u and w spectra at four heights above the canopy, plotted against frequency n. The spectra collapse with no scaling, or (equivalently) when plotted against the dimensionless frequency $f = nL_s/U_A$ where the length scale L_s and the advection velocity U_A are constant or everywhere proportional to one another. The collapse is particularly striking for the u spectra. Both spectra appear much more scattered when plotted with the inertial-sublayer scaling $f = n(z - d)/\bar{u}(z)$, which is not surprising given the absence of a well-developed inertial sublayer in the present experiment.

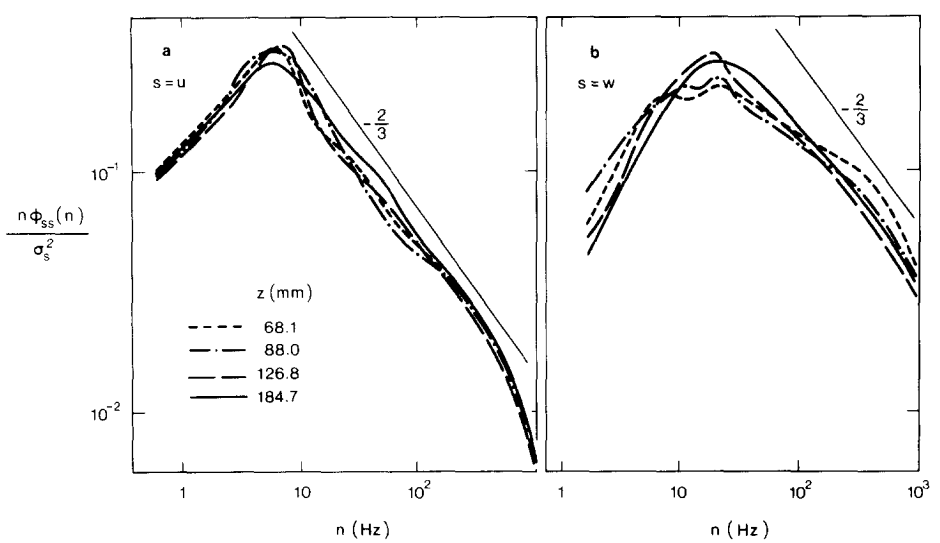

Fig. 11. Above-canopy spectra for (a) u; (b) w. Measurements at position D, $x = 2.47$ m.

One interpretation of the spectral collapse against n(or nL_s/U_A) is to consider the spectra the result of a population of large, long-lived, coherent eddies with a mean streamwise spacing (L_s) proportional to the boundary-layer depth δ, and an advection velocity U_A which is independent of height, despite the existence of a mean shear. The

idea that $L_s \propto \delta$ underlies the concept of mixed-layer scaling for the unstable atmospheric boundary layer, where the u-spectrum peak wavelength is found to be 1.5 δ and height-independent (Kaimal, 1978). If L_s is assumed independent of z in our experiment, then U_A must be also because of the scaling demonstrated in Figure 11. A rough estimate of U_A is the average of $\langle \bar{u} \rangle(z)$ between h_c and δ, about 8 m s^{-1} in our case. The u and w spectra in Figure 11 have peak frequencies (n_p) of 6 and 20 Hz, respectively, corresponding to peak wavelengths (U_A/n_p) of 2.3 δ for the u spectrum and 0.7 δ for the w spectrum.

For the inertial subrange, the Kolmogorov hypotheses predict the spectral densities of u and w (ϕ_{uu} and ϕ_{ww}, respectively) to be

$$n\phi_{uu}(n) = \alpha_u \varepsilon^{2/3} (2\pi n/\bar{u})^{-2/3}$$
$$n\phi_{ww}(n) = \alpha_w \varepsilon^{2/3} (2\pi n/\bar{u})^{-2/3} \tag{21}$$

where ε is the dissipation rate, and α_u and α_w are constants. The assumption of local isotropy gives $\alpha_w = 4\alpha_u/3$, while many empirical determinations give $\alpha_u \approx 0.5$ (Monin and Yaglom, 1975). The Taylor 'frozen turbulence' hypothesis has been assumed in the usual way for the small eddies in the inertial subrange. The u and w spectra both exhibit some inertial subrange with the required $-2/3$ slope, except for the w spectrum just above the canopy, which shows wake influence (see below). The rolloff in the spectra above 500 Hz is caused by the low-pass filtering of the signals.

Spectra of u and w within the canopy are shown in Figure 12. No dimensionless frequency f can be found to collapse the data. The reason is most clear from the w spectrum, where two peaks are evident: a low-frequency peak at $n \approx 20$ Hz, closely related to the peak in the w spectrum above the canopy, and a higher frequency peak at $n \approx 100$ Hz, which becomes progressively more dominant as z/h_c decreases. This result is consistent with the idea that canopy momentum transfer is dominated by gust motions associated with larger-scale coherent eddies above the canopy. As the gusts move downwards through the canopy, they progressively transfer their energy from large (boundary-layer) to small (element-wake) scales, through the action of form drag by the canopy elements (Raupach and Shaw, 1982). In such a situation, at least two length scales are significant in the spectra, to different extents at different heights, so that no single length scale can be found. The u spectra also show a shift towards a higher-frequency peak as z/h_c decreases, though it is less pronounced than for the w spectra because the low-frequency energy is much higher for u than for w. Thus, the low-frequency component remains more dominant within the canopy.

The cospectrum of uw is shown in Figure 13 in area-preserving (rather than log-log) form, at four heights within and one above the canopy. (As for the spectra, uw cospectra collapse well above the canopy, so only one example suffices). Not surprisingly, the peak frequency of the uw cospectrum is similar to that of the u spectrum. However, the unexpected feature of the cospectrum is the change in sign at high frequencies, especially at mid-canopy levels (z = 29.0 and 45.7 mm). At the lowest level (z = 13.1 mm) the cospectrum is everywhere positive, consistent with the observed positive $\overline{u'w'}$ value

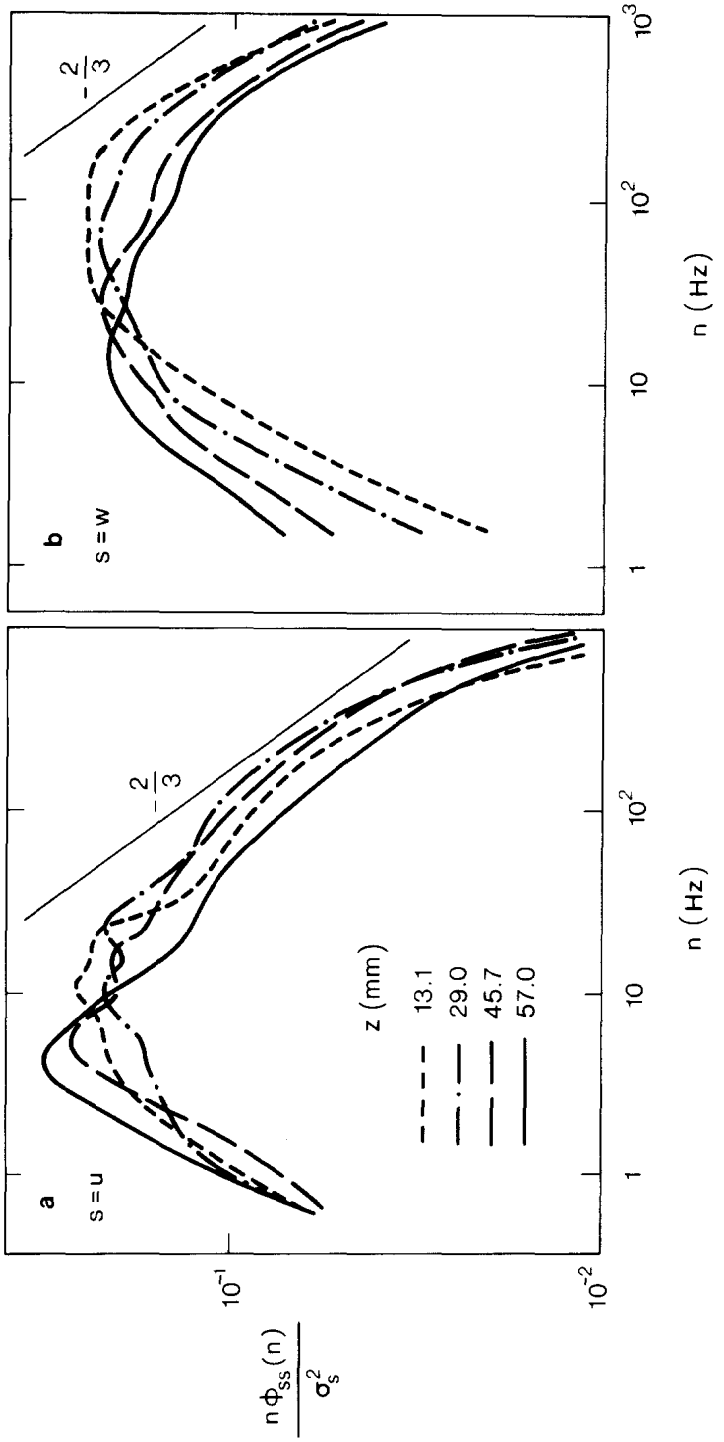

Fig. 12. Within-canopy spectra for (a) u; (b) w. Measurements at position D, $x = 2.47$ m.

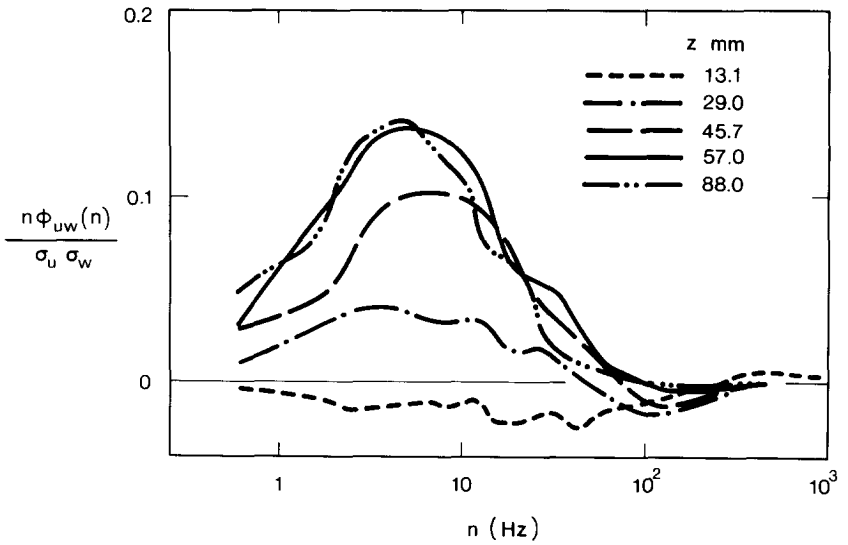

Fig. 13. Cospectra for uw. Measurements at position D, x = 2.47 m.

there (see section 4.2). Although these results must be viewed with great caution because of the three-wire probe uncertainties associated with high-intensity turbulence, it is possible that they are substantially correct and are associated with systematic recirculations in element wakes, as discussed earlier.

For comparison between this and similar experiments, it is wothwhile to compute the Eulerian turbulent length scales L_{Ew} and L_{Eu}, defined by

$$L_{Ew} = \frac{\bar{u}}{\sigma_w^2} \int_0^{\tau_1} \overline{w'(t)w'(t+\tau)}\, d\tau$$
$$L_{Eu} = \frac{\bar{u}}{\sigma_u^2} \int_0^{\tau_1} \overline{u'(t)u'(t+\tau)}\, d\tau \qquad (22)$$

where τ_1 is the time lag for the first zero crossing of the autocovariance function. These scales, especially L_{Ew}, have been suggested as turbulence-derived scales relevant to scalar dispersion within the canopy (Wilson *et al.*, 1982). Figure 14 shows L_{Ew} and L_{Eu} for our data, in comparison with the results of Wilson *et al.* (1982) from a corn canopy and Seginer *et al.* (1976) from a model canopy of vertical rods. Our measurements are consistent in form with the behaviour of K_M (Figure 10) but are higher than those of both Wilson *et al.* (1982) and Seginer *et al.* (1976).

8. Budgets for Turbulent Energy and Shear Stress

8.1. The turbulent energy budget

For the conditions of our experiment (a stationary flow with no buoyancy forces and

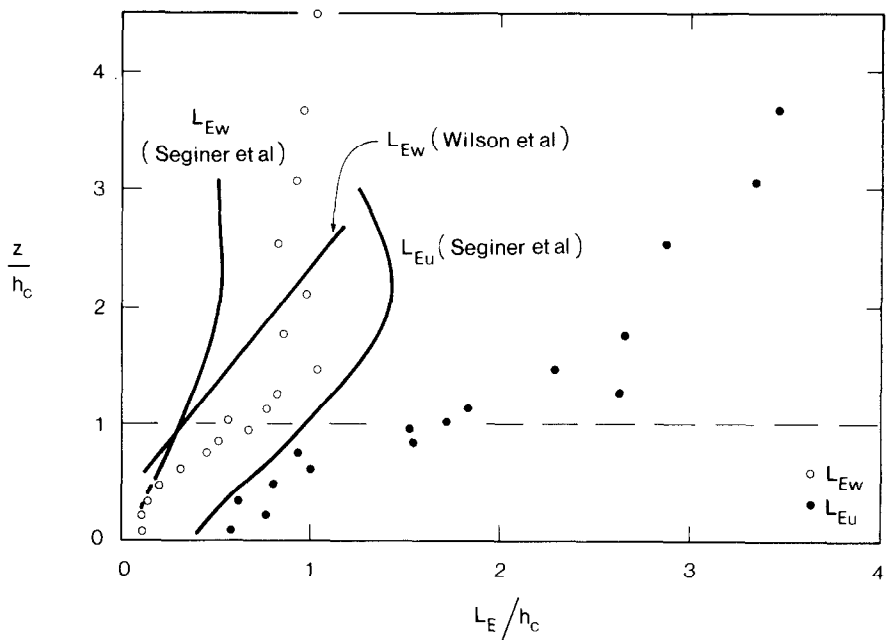

Fig. 14. The length scales L_{Ew} and L_{Eu}, defined by Equation (22).

no mean streamwise evolution, over and through a canopy with rigid elements), the spatially averaged turbulent energy budget simplifies to

$$\frac{1}{2}\frac{\partial\langle\overline{q^2}\rangle}{\partial t} = \underbrace{-\langle\overline{u'w'}\rangle\frac{\partial\langle\overline{u}\rangle}{\partial z}}_{P_s} \underbrace{-\left\langle\overline{u_i'u_j'}''\frac{\partial\overline{u}_i''}{\partial x_j}\right\rangle}_{P_w} \underbrace{-\frac{\partial}{\partial z}\left\langle\frac{\overline{w'q^2}}{2}\right\rangle}_{T_t} \underbrace{-\frac{\partial}{\partial z}\left\langle\frac{\overline{w}''\overline{q^2}''}{2}\right\rangle}_{T_d}$$

$$\underbrace{-\frac{\partial}{\partial z}\langle\overline{p'w'}\rangle}_{T_p} + \underbrace{\nu\frac{\partial^2}{\partial z^2}\left\langle\frac{\overline{q^2}}{2}\right\rangle}_{T_m} - \underbrace{\langle\varepsilon\rangle}_{D}, \tag{23}$$

where $\overline{q^2} = \overline{u_i'u_i'}$ is twice the turbulent energy and ε is the dissipation rate $\nu\overline{(\partial u_i'/\partial x_j)(\partial u_i'/\partial x_j)}$. Tensor notation is used where convenient. P_s is shear production; P_w wake production; T_t, T_d, T_p and T_m the turbulent, dispersive, pressure and molecular transport terms, respectively, and D the dissipation. All these terms are familiar from conventional above-canopy analyses except P_w and T_d; T_d is directly analogous to the dispersive momentum flux divergence in Equation (8), while P_w accounts for the conversion of mean kinetic energy to turbulent energy in element wakes by working of the mean flow against drag. It can be shown that

$$-P_w = \left\langle\overline{u_i'u_j'}''\frac{\partial\overline{u}_i''}{\partial x_j}\right\rangle = \langle\overline{u}_i\rangle(f_{Fi} + f_{Vi}) \tag{24}$$

provided that (1) there is negligible direct dissipation by the canopy of mean kinetic energy to heat (without prior conversion to wake turbulence), and (2) the dispersive stress $\langle \bar{u}_i'' \bar{u}_j'' \rangle$ and the dispersive flux of kinetic energy are both negligible (Raupach and Shaw, 1982)*. Physically, (2) means that the turbulent energy arising from work against drag on elements within an averaging volume is produced within the same averaging volume. We have shown that $\langle \bar{u}'' \bar{w}'' \rangle$ is negligible, at least for $z \gtrsim h_c$, and will extend this by assuming that the necessary dispersive fluxes vanish so that Equation (24) holds everywhere. Equations (24) and (12) (with the assumption that dispersive and molecular contributions to the shear stress are negligible) give

$$-P_w = \left\langle \overline{u_i' u_j'}'' \frac{\partial \bar{u}_i''}{\partial x_j} \right\rangle = \langle \bar{u} \rangle \frac{\partial \langle \overline{u' w'} \rangle}{\partial z}, \tag{25}$$

which enables the wake production term to be evaluated in practice.

Figure 15(a) shows measurements (at $x = 2.47$ m) of P_s, P_w, T_t and D ($= -\langle \varepsilon \rangle$). Two different measurements of D are shown. The dots denote values from the inertial subrange u and w spectra, assuming $\alpha_u = 0.5$; see Equation (21) and Figures 11 and 12. The broken line denotes the residual $-P_s - P_w - T_t$. which is equal to D if T_d, T_p and T_m are all negligible; of these, T_m is certainly negligible, T_d is small at least for $z \gtrsim h_c$ (by analogy with the dispersive momentum flux) and T_p is considered below. Note also that the assumption of no mean streamwise evolution, used to eliminate terms involving mean streamwise derivatives from Equation (23), was checked by measuring the terms for advection and streamwise turbulent transport. Both were negligible.

Shear production and wake production both have strong peaks, of comparable magnitude, near $z = h_c$. Unlike an equilibrium surface layer, where production is approximately balanced by dissipation, there is a large downward turbulent transport of turbulent energy into the canopy, T_t being a loss near $z = h_c$ of about one third of the combined production terms. Dissipation is highest at about $z = 0.8\, h_c$, but remains significant in the lower part of the canopy where it is balanced mainly by transport from above. These general features agree remarkably well with the second-order closure predictions of Wilson and Shaw (1977).

The residual and spectral measurements of $\langle \varepsilon \rangle$ show fair agreement within the canopy, but there an inertial subrange cannot be assumed because of high-frequency wake production. Therefore, this agreement cannot be taken as significant. Just above the canopy, however, there is a discrepancy of a factor of two between the two measurements of $\langle \varepsilon \rangle$, which we believe to be greater than can be accounted for by known errors of assumption or measurement. If the discrepancy is, in fact, real, it implies significant pressure transport in the $\overline{q^2}/2$ budget for z between about h_c and $2\, h_c$, such that T_p roughly balances the loss due to T_t.

The result that T_t is significant over rough surfaces is not new (Maitani, 1979;

* Raupach and Shaw omitted f_{Vi} from Equation (24) (their Equation (17)), equating direct dissipation by the canopy, of mean kinetic energy to heat, with working of the mean flow against viscous drag. This is not true in general.

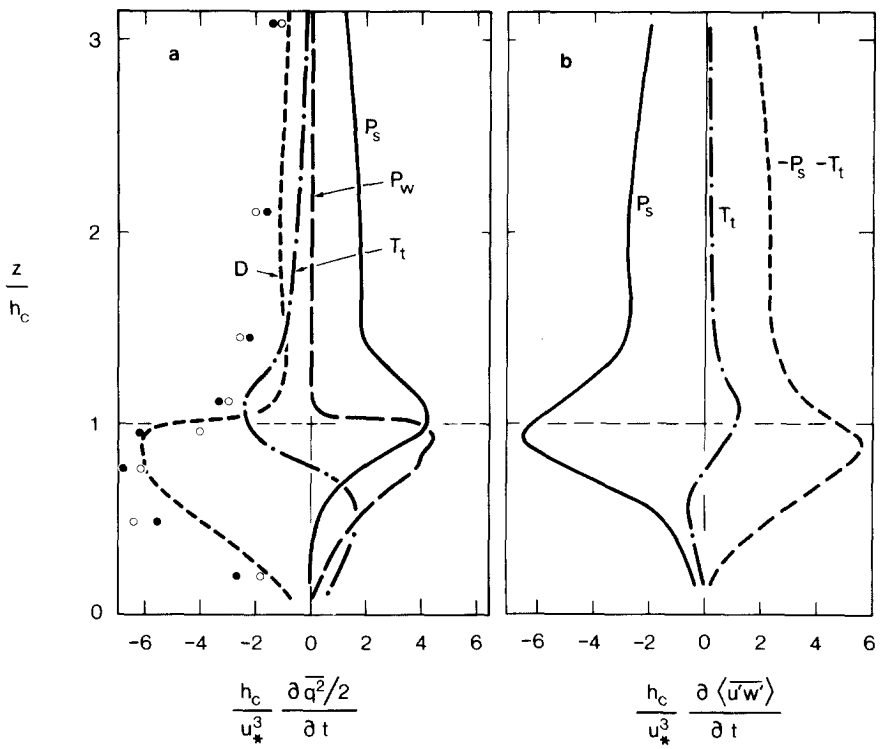

Fig. 15. (a) The turbulent energy budget at x = 2.47 m. Open circles, dissipation from u spectrum; closed circles, dissipation from x spectrum. (b) The shear stress budget at x = 2.47 m.

Andreopoulos and Bradshaw, 1981; Raupach, 1981). However, our budget result implies that, for z between h_c and 2 h_c, the combination of T_t and T_p is much smaller than T_t alone. Therefore, the flow just above the canopy is in approximate local equilibrium (production balancing dissipation), as also observed in neutral and unstable atmospheric surface layers well above the roughness (Bradley *et al.*, 1981). Note that the local equilibrium cannot extend far into the canopy. If we interpret literally our observed discrepancy between spectral and residual measurements of dissipation in the lower part of the canopy, despite the cautions above, the implication is that both T_t and T_p are positive.

8.2. The shear stress budget

For the same conditions as for Equation (23), the spatially-averaged shear-stress budget is

$$\frac{\partial \langle \overline{u'w'} \rangle}{\partial t} = 0 = -\langle \overline{w'^2} \rangle \frac{\partial \langle \bar{u} \rangle}{\partial z} - \left\langle \overline{u_1' u_j''} \frac{\partial \bar{u}_3''}{\partial x_j} + \overline{u_3' u_j''} \frac{\partial \bar{u}_1''}{\partial x_j} \right\rangle$$

$$\begin{matrix} P_s & & P_w \\ -\frac{\partial}{\partial z}\langle\overline{u'w'^2}\rangle - \frac{\partial}{\partial z}\langle\overline{w}''\overline{u'w'}''\rangle - \frac{\partial}{\partial z}\langle\overline{p'u'}\rangle \\ T_t & T_d & T_p \\ + \nu\frac{\partial^2}{\partial z^2}\langle\overline{u'w'}\rangle + \left\langle\overline{p'\left(\frac{\partial u'}{\partial z}+\frac{\partial w'}{\partial x}\right)}\right\rangle - 2\nu\left\langle\frac{\partial u_1'}{\partial x_j}\frac{\partial u_3'}{\partial x_j}\right\rangle, \\ T_m & \Phi & D \end{matrix} \quad (26)$$

where terms correspond in name and mnemonic with Equation (23) except for the pressure-strain term, Φ, which is the dominant destruction term for the shear stress since molecular dissipation (D) is small (Wyngaard *et al.*, 1971). Other terms which are probably small in Equation (26) are dispersive flux divergence (T_d), molecular flux divergence (T_m) and wake production (P_w). The negligibility of P_w follows from the equation

$$\left\langle\overline{u_i'u_j'}''\frac{\partial\overline{u}_k''}{\partial x_j} + \overline{u_k'u_j'}\frac{\partial\overline{u}_i''}{\partial x_j}\right\rangle = \langle\overline{u}_i\rangle(f_{Fk}+f_{Vk}) + \langle\overline{u}_k\rangle(f_{Fi}+f_{Vi}) \quad (27)$$

which is a tensor generalization of Equation (24), valid under the same constraints and derivable by the same method. When $i = 1$ and $k = 3$, as in the shear stress budget, the right-hand side of Equation (27) becomes negligible because $f_{F3} + f_{V3}$ (vertical drag) and $\langle\overline{u}_3\rangle$ are both negligible.

Figure 15(b) shows measurements at $x = 2.47$ m of P_s and T_t in Equation (26), together with the residual $-P_s - T_t$, equal to $T_p + \Phi$ if other terms are small. As with the turbulent energy budget, shear production peaks strongly near $z = h_c$, while turbulent transport is a loss near $z = h_c$ and a gain lower down. However, the role of transport in the shear stress budget is relatively smaller than in the turbulent energy budget. This can be understood thus: just above $z = h_c$, the ratio of the shear production terms in the shear stress and turbulent energy budgets is $|\langle\overline{w'^2}\rangle/\langle\overline{u'w'}\rangle| = 1.6$, whereas the ratio of the fluxes responsible for turbulent transport in the two budgets is $|\langle\overline{u'w'^2}\rangle/\langle\overline{w'q'^2}/2\rangle| = 0.2$. Since the flux of shear stress is relatively so much smaller than the flux of turbulent energy while shear production rates are comparable, it is likely that turbulent transport (the vertical gradient of the flux) will be of less importance for shear stress than for turbulent energy.

Our results for the shear stress budget, as for the turbulent energy budget, agree well with the model predictions of Wilson and Shaw (1977).

9. Conditional Statistics of the Shear Stress

The technique of 'quadrant-hole analysis' (Lu and Willmarth, 1973) enables some information about the structure of turbulent transport to be deduced from turbulence measurements at a single point. It was used by Finnigan (1979b) in a field investigation of momentum transfer to a waving wheat canopy, by Shaw *et al.* (1983) in a similar study for a relatively inflexible corn canopy, and by Raupach (1981) in a laboratory investigation of the effect of roughness density on the momentum transfer process close to a rough surface. These studies all showed that, within the canopy, most of the momentum transfer occurs during short, intermittent gusts or sweeps. Here we present briefly a similar analysis for the present experiment.

The four quadrants (i) in the $u'w'$ plane are conventionally labelled as outward interactions ($i = 1; u' > 0, w' > 0$), ejections ($i = 2; u' < 0, w' > 0$), inward interactions ($i = 3; u' < 0, w' < 0$) $s_{i,H}$ and sweeps ($i = 4; u' > 0, w' < 0$). We consider $u'(t)$ and $w'(t)$ at a single point and define the normalized conditional stress $s_{i,H}$ as

$$s_{i,H} = \frac{1}{\sigma_u \sigma_w T} \int_0^T u'(t) w'(t) I_{i,H}(u', w') \, dt, \tag{28}$$

where $I_{i,H}(u', w')$ is an indicator function which is 1 when $(u'(t), w'(t))$ is in the i^{th} quadrant and when $|u'(t)w'(t)|$ is greater than $H\sigma_u\sigma_w$, and zero otherwise. The parameter H, the 'hole size', sets a hyperbolic exclusion zone in the $u'w'$ plane. Hence, $s_{i,H}$ is the stress contribution, normalized by $\sigma_u\sigma_w$, arising from periods when the vector $(u'(t), w'(t))$ is in quadrant i and the instantaneous stress $|u'(t)w'(t)|$ is greater than $H\sigma_u\sigma_w$. The time fraction during which the stress contribution $s_{i,H}$ is being made is

$$t_{i,H} = \frac{1}{T} \int_o^T I_{i,H}(u', w') \, dt. \tag{29}$$

When $H = 0$, so that there is no exclusion zone, we have

$$\sum_{i=1}^{4} s_{i,0} = r_{uw}, \quad \sum_{i=1}^{4} t_{i,0} = 1, \tag{30}$$

where r_{uw} is the correlation coefficient $\overline{u'w'}/\sigma_u\sigma_w$. Note that we have normalized both $s_{i,H}$ and H with $\sigma_u\sigma_w$ (following Lu and Willmarth, 1973) rather than with $\overline{u'w'}$ (following the canopy studies mentioned above). This is necessary to permit comparison between flow regions of very different r_{uw}.

Figure16 shows $s_{i,H}$ plotted against H for three heights within and one just above the canopy, while Table III gives related information, including the correlation coefficients r_{uw}. Just above the canopy ($z/h_c = 1.13$), the ejection ($i = 2$) and sweep ($i = 4$) quadrants make approximately equal contributions to the shear stress at all hole sizes H, with much smaller and similarly symmetric contributions from the interaction quadrants ($i = 1, 3$). This behaviour is characteristic of a strongly negatively correlated joint Gaussian probability density function (pdf) for u' and w'; the measured r_{uw} of -0.47, and the

skewnesses and kurtoses at this level, are consistent with this. An approximately joint Gaussian pdf for u' and w' and a shear stress which is not biased towards either ejections or sweeps are properties of the neutrally stratified inertial sublayer (Raupach, 1981). Also, the transport process is quite intermittent; half the momentum transfer occurs when $H > 1.7$, yet this transfer occurs only 10% of the time.

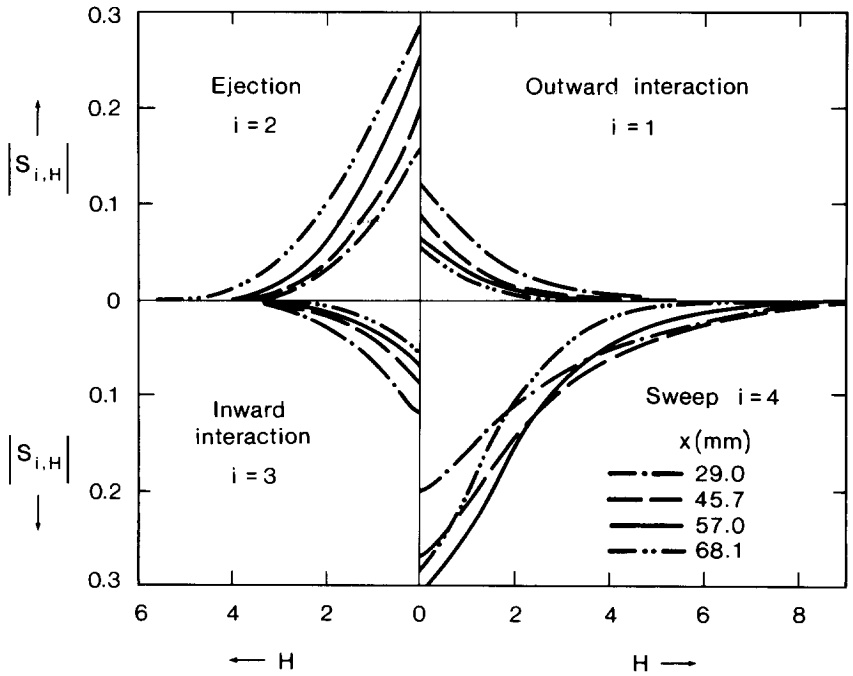

Fig. 16. Stress fractions $s_{i,H}$ plotted against hole size H. Measurements at position D, x = 2.47 m.

Within the canopy, sweeps contribute more to momentum transfer than ejections, evident from the values in Table III of $s_{4,0}/s_{2,0}$, the ratio of momentum transfer by all sweeps to that by all ejections, irrespective of hole size. This ratio is almost 1.3 in the upper half of the canopy where most of the momentum is absorbed. However, the importance of sweeps becomes even greater when attention is restricted to the more intense events contributing to the stress. This can be done by defining the hole size H′ above which half the momentum transfer occurs:

$$\sum_{i=1}^{4} s_{i,H'} = r_{uw}/2 \,. \tag{31}$$

Table III shows H' and $s_{4,H'}/s_{2,H'}$, the ratio of momentum transfer by sweeps to that by ejections when only the stronger events (those outside the exclusion zone defined by H') are considered. Intense sweeps are far more important than intense ejections within

TABLE III

Parameters pertaining to the quadrant-hole analysis in Figure 16

z (mm)	29	46	57	68
z/h_c	0.48	0.76	0.95	1.13
r_{uw}	−0.11	−0.31	−0.43	−0.47
H'	2.7	2.0	1.8	1.7
$s_{4,0}/s_{2,0}$	1.20	1.31	1.22	1.00
$s_{4,H'}/s_{2,H'}$	6.45	3.26	2.16	1.02
$\sum_{i=1}^{4} t_{i,H'}$	0.032	0.070	0.106	0.103

the canopy, and their dominance increases with decreasing height. Furthermore, the entire momentum transfer process becomes more intermittent; the total time fraction occupied by the more intense events diminishes as z/h_c decreases, as shown in Table III. At $z/h_c = 0.48$, half the momentum transfer occurs in only 3% of the time.

These features agree broadly with the findings of Finnigan (1979b), Raupach (1981) and Shaw *et al.* (1983), though with two significant points of disagreement in detail. Firstly, equality between sweep and ejection contributions to $\overline{u'w'}$ above the canopy occurs as low as $z/h_c = 1.13$ in this experiment, whereas Raupach (1981) found equality at $z/h_c \approx 4$. This is another indication of the fact that h_c/δ in our experiment is too large to allow the formation of a well-defined inertial sublayer in which the pdf for u' and w' is close to joint Gaussian. Instead, this region is 'squeezed' between the sweep-dominated roughness sublayer and the ejection-dominated outer layer.

Secondly, the extent of sweep domination within the canopy, as measured by $s_{4,0}/s_{2,0}$, is less in the present work than in any of the other three studies. (We find $s_{4,0}/s_{2,0} \approx 1.3$; Shaw *et al.* (1983) found about 2, the other studies higher still.) Two factors explain this difference: firstly, we used a three-wire probe for the velocity measurements whereas Finnigan (1979b) and Raupach (1981) both used X-wires. Another paper (Coppin and Raupach, 1986) will show that X-wires can cause severe overestimates of $s_{4,0}/s_{2,0}$ and other similar parameters of the quadrant-hole analysis when used in high-intensity turbulence. This is likely to account for much of the difference between the present work and the results of Finnigan and Raupach. The other factor is the absence of a well-defined inertial sublayer in this experiment, which probably meant that the turbulence structure in our canopy was influenced somewhat by the outer layer and was therefore less biased towards sweeps than it would have been if an inertial sublayer had existed. Since the outer layer is ejection-dominated (Raupach, 1981), it is reasonable to suppose that an inadequate inertial sublayer 'buffer' between the outer layer and the canopy will reduce the extent of sweep dominance within the canopy.

10. Conclusions

A fairly complete picture now exists of the structure of turbulence in a uniform, neutrally stratified, nonwaving plant canopy, at least as far as single-point statistics are concerned. Spectra show the importance of eddies larger than the canopy itself. As the ground is approached these eddies become increasingly asymmetric in the sense that the joint pdf of u' and w' becomes increasingly nonGaussian. This has several related consequences (Raupach, 1981): (i) the third moments of u' and w' become large, with the u skewness strongly positive and the w skewness strongly negative; (ii) turbulent transport is crucial in the turbulent energy budget and (to a lesser extent) in the shear stress budget; and (iii) sweeps account for more shear stress within the canopy than ejections. The main contributions of the present work to this picture are (i) the measurement of turbulent energy and shear stress budgets, especially the wake production and turbulent transport terms; (ii) the quantification of the dispersive momentum flux, which turns out to be practically negligible, at least for $z \gtrsim h_c$; and (iii) the reappraisal of the behaviour of shear stress within the canopy under quadrant analysis. This was made possible by the three-wire probe, and shows that earlier work with X-wires overstated the extent to which the sweep quadrant dominates momentum transport. However, the reappraisal does not change the essential picture.

There are two main areas for further work. Firstly, more measurements – including direct ones (Sigmon *et al.*, 1983) – are needed on the role of pressure fluctuations. Our data suggest that pressure transport cancels turbulent transport in the turbulent energy budget just above the canopy, a result which needs confirmation and extension. Secondly, multipoint statistics, both conventional and conditional, are needed to round out the picture offered by single-point measurements.

References

Andreopoulos, J. and Bradshaw, P.: 1981, 'Measurements of Turbulence Structure in the Boundary Layer on a Rough Surface', *Boundary-Layer Meteorol.* **20**, 201–213.

Bradley, E. F., Antonia, R. A., and Chambers, A. J.: 1981, 'Turbulence Reynolds Number and the Turbulent Kinetic Energy Balance in the Atmospheric Surface Layer', *Boundary-Layer Meteorol.* **21**, 183–197.

Bradshaw, P.: 1967, "Inactive' Motion and Pressure Fluctuations in Turbulent Boundary Layers', *J. Fluid Mech.* **30**, 241–258.

Coppin, P. A. and Raupach, M. R.: 1986, 'An Evaluation of Quadrant Analysis of Momentum and Scalar Fluxes Close to Rough Surfaces', *Boundary-Layer Meteorol.* (to be submitted).

Coppin, P. A., Raupach, M. R., and Legg, B. J.: 1986, 'Experiments on Scalar Dispersion within a Model Canopy, Part II: An Elevated Plane Source', *Boundary-Layer Meteorol.* **35**, 167–191.

Coppin, P. A. and Taylor, K. J.: 1983, 'A Three-Component Sonic Anemometer-Thermometer System for General Micrometeorological Research', *Boundary-Layer Meteorol.* **27**, 27–42.

Corrsin, S.: 1974, 'Limitations of Gradient Transport Models in Random Walks and in Turbulence', *Adv. Geophys.* **18A**, 25–60.

Fackrell, J. E. and Robins, A. G.: 1982, 'Concentration Fluctuations and Fluxes in Plumes from Point Sources in a Turbulent Boundary Layer', *J. Fluid Mech.* **117**, 1–26.

Finnigan, J. J.: 1979a, 'Turbulence in Waving Wheat. I. Mean Statistics and Honami', *Boundary-Layer Meteorol.* **16**, 181–211.

Finnigan, J. J.: 1979b, 'Turbulence in Waving Wheat. II. Structure of Momentum Transfer', *Boundary-Layer Meteorol.* **16**, 213–236.

Finnigan, J. J.: 1985, 'Turbulence Transport in Flexible Plant Canopies', in B. A. Hutchison and B. B. Hicks (eds.), *The Forest Atmosphere Interaction*, pp. 443–480, D. Reidel Publishing Co., Dordrecht, The Netherlands.

Finnigan, J. J. and Raupach, M. R.: 1986, 'Transfer Processes in Plant Canopies in Relation to Stomatal Characteristics', in E. Zeiger, G. Farquhar and I. Cowan (eds.), *Stomatal Function*, Stanford University Press, Stanford, CA, U.S.A. (in press).

Jackson, P. S.: 1981, 'On the Displacement Height in the Logarithmic Velocity Profile'. *J. Fluid Mech.* **111**, 15–25.

Hoerner, S. J.: 1965, *Fluid-Dynamic Drag*, published by the author.

Kaimal, J. C.: 1978, 'Horizontal Velocity Spectra in an Unstable Surface Layer', *J. Atmos. Sci* **35**, 18–24.

Legg, B. J.: 1983, 'Turbulent Diffusion from an Elevated Line Source: Markov Chain Simulations of Concentration and Flux Profiles', *Quart. J. Roy. Meteorol. Soc.* **109**, 645–660.

Legg, B. J., Coppin, P. A., and Raupach, M. R.: 1984, 'A Three-Hot-Wire Anemometer for Measuring Two Velocity Components in High Intensity Turbulent Boundary Layers', *J. Phys. E.* **17**, 970–976.

Legg, B. J., Raupach, M. R., and Coppin, P. A.: 1986, 'Experiments on Scalar Dispersion Within a Model Plant Canopy, Part III: An Elevated Line Source', *Boundary-Layer Meteorol.* (in press).

Lu, S. S. and Willmarth, W. W.: 1973, 'Measurements of the Structure of the Reynolds Stress in a Turbulent Boundary Layer', *J. Fluid Mech.* **60**, 481–571.

Maitani, T.: 1979, 'A Comparison of Turbulence Statistics in the Surface Layer over Plant Canopies with Those over Several Other Surfaces', *Boundary-Layer Meteorol.* **17**, 213–222.

Monin, A. S. and Yaglom, A. M.: 1975, *Statistical Fluid Mechanics: Mechanics of Turbulence*, Vol. 2, MIT Press, Cambridge, Mass., U.S.A. Eng. Trans. J. L. Lumley (ed.), 874 pp.

Mulhearn, P. J.: 1978, 'Turbulent Flow over a Periodic Rough Surface', *Phys. Fluids* **21**, 1113–1115.

Mulhearn, P. J. and Finnigan, J. J.: 1978, 'Turbulent Flow over a Very Rough, Random Surface', *Boundary-Layer Meteorol.* **15**, 109–132.

Panofsky, H. A.: 1974, 'The Atmospheric Boundary Layer Below 150 m', *Ann. Rev. Fluid Mech.* **6**, 147–177.

Raupach, M. R.: 1981, 'Conditional Statistics of Reynolds Stress in Rough-Wall and Smooth-Wall Turbulent Boundary Layers', *J. Fluid Mech.* **108**, 363–382.

Raupach, M. R. and Shaw, R. H.: 1982, 'Averaging Procedures for Flow within Vegetation Canopies', *Boundary-Layer Meteorol.* **22**, 79–90.

Raupach, M. R. and Legg, B. J.: 1983, 'Turbulent Dispersion from an Elevated Line Source: Measurements of Wind-Concentration Moments and Budgets', *J. Fluid Mech.* **136**, 111–137.

Raupach, M. R., Thom, A. S., and Edwards, I.: 1980, 'A Wind Tunnel Study of Turbulent Flow Close to Regularly Arrayed Rough Surfaces', *Boundary-Layer Meteorol.* **18**, 373–397.

Rouse, H. (ed.): 1959, *Advanced Mechanics of Fluids*, Wiley, New York, 444 pp.

Seginer, I. and Mulhearn, P. J.: 1978, 'A Note on Vertical Coherence of Streamwise Turbulence Inside and Above a Model Plant Canopy', *Boundary-Layer Meteorol.* **14**, 515–523.

Seginer, I., Mulhearn, P. J., Bradley, E. F., and Finnigan, J. J.: 1976, 'Turbulent Flow in a Model Plant Canopy', *Boundary-Layer Meteorol.* **10**, 423–453.

Shaw, R. H., Tavangar, J., and Ward, D. P.: 1983, 'Structure of the Reynolds Stress in a Canopy Layer', *J. Climate Appl. Meteorol.* **22**, 1922–1931.

Sigmon, J. T., Knoerr, K. R., and Shaughnessy, E. J.: 1983, 'Microscale Pressure Fluctuations in a Mature Deciduous Forest, *Boundary-Layer Meteorol.* **27**, 345–358.

Thom, A. S.: 1971, 'Momentum Absorption by Vegetation', *Quart. J. Roy. Meteorol. Soc.* **97**, 414–428.

Wilson, J. D., Ward, D. P., Thurtell, G. W., and Kidd, G. E.: 1982, 'Statistics of Atmospheric Turbulence within and above a Corn Canopy', *Boundary-Layer Meteorol.* **24**, 495–519.

Wilson, N. R. and Shaw, R. H.: 1977, 'A Higher-Order Closure Model for Canopy Flow', *J. Appl. Meteorol.* **16**, 1198–1205.

Wooding, R. A.: 1968, 'A Low Speed Wind Tunnel for Model Studies in Micrometeorology. II. The Pye Laboratory Wind Tunnel.' *Aust. CSIRO Div. Plant Ind. Tech. Pap.* No. 25, pp. 25–39.

Wyngaard, J. C., Coté, O. R., and Izumi, Y.: 1971, 'Local Free Convection, Similarity, and the Budgets of Shear Stress and Heat Flux', *J. Atmos. Sci.* **28**, 1171–1182.